

MIT Open Access Articles

Selective fluoride removal from groundwater using CNT-CeO₂ electrodes in capacitive deionization (CDI)

The MIT Faculty has made this article openly available. **Please share** how this access benefits you. Your story matters.

Citation: Liu, Xun, Rehman, Danyal, Shu, Yufei, Liu, Bei, Wang, Li et al. 2024. "Selective fluoride removal from groundwater using CNT-CeO₂ electrodes in capacitive deionization (CDI)." Chemical Engineering Journal, 482.

As Published: 10.1016/j.cej.2024.149097

Publisher: Elsevier BV

Persistent URL: <https://hdl.handle.net/1721.1/155273>

Version: Author's final manuscript: final author's manuscript post peer review, without publisher's formatting or copy editing

Terms of use: Creative Commons Attribution-Noncommercial-ShareAlike



Selective Fluoride Removal from Groundwater Using CNT-CeO₂ Electrodes in Capacitive Deionization (CDI)

Xun Liu^{ab#}, Danyal Rehman^{cd#}, Yufei Shu^b, Bei Liu^b, Li Wang^b, Li Li^b, Mengxia Wang^{ab}, Kunkun Wang^b, Qi Han^b, Linlin Zang^b, John H. Lienhard^{c*}, Zhongying Wang^{b*}

^a School of Environment, Harbin Institute of Technology, PR China

^b School of Environmental Science and Engineering, Southern University of Science and Technology, Shenzhen 518055, PR China

^c Department of Mechanical Engineering, Massachusetts Institute of Technology, Cambridge, MA 02139, United States of America

^d Center for Computational Science and Engineering, Massachusetts Institute of Technology, Cambridge, MA 02139, United States of America

Corresponding authors:

Zhongying Wang, email: wangzy6@sustech.edu.cn; tel.: +86-075588018040;

John H. Lienhard, email: lienhard@mit.edu; tel.: +1-617-253-3790.

[#] These authors contributed equally to this work.

Abstract

Selective capacitive deionization (SCDI) is a promising process for preferentially removing specific ions from waters with complex compositions. The selectivity towards certain species in CDI is most frequently achieved through novel electrode materials with high affinities towards targeted species. In this study, we investigate the selective removal of fluoride ions from groundwater containing concentrated co-existing chloride ions. A carbon nanotube-CeO₂ (CNT-CeO₂) electrode is employed for the electro-sorption of fluoride ions. Our findings are compelling: when processing a mixed F⁻/Cl⁻ solution comprising 10 mg/L F⁻ and 100 mg/L Cl⁻, the CNT-CeO₂ electrode is seen to reduce the concentration of F⁻ ions to 1.5 mg/L in just 150 min, amounting to an 85% F⁻ removal efficiency, while the Cl⁻ removal efficiency remains below 2%. Importantly, this translates to a F⁻/Cl⁻ separation factor of up to 4.16 when using the CeO₂-based electrodes, which is 40 times higher than that achieved with conventional activated carbon (AC) electrodes. Furthermore, the energy consumption for treating actual groundwater using scaled-up equipment is impressively low at approximately 0.2 kWh/m³. The high affinity of CNT-CeO₂ towards fluoride is attributed to the intercalation Faraday capacitance initiated by the reaction between F⁻ with CeO₂, as verified by the electrochemical quartz crystal microbalance (EQCM). Moreover, EQCM results show a substantial increase in both mass and current as the potential increased beyond 0.8 V vs Ag/AgCl, implying that the current surge is not a result of water splitting but rather the adsorption of F⁻ onto the CNT-CeO₂ electrode. The addition of CNTs substantially increases the conductivity of CeO₂ electrodes and restricts the aggregation of CeO₂, thereby accelerating ion diffusion and promoting selective adsorption characteristics. Importantly, our electro-driven approach demonstrates excellent adsorption-desorption over 20 cycles. This comprehensive study advances the technological development of selective CDI, while providing new insights for fluoride removal in groundwater.

Keywords: selective capacitive deionization, defluoridation, cerium dioxide, carbon nanotubes, selective separations

1. Introduction

Fluoride (F^-), an essential mineral found in various sourcewaters globally, plays a critical role in human health [1]. Despite its benefits, prolonged exposure to high concentrations of fluoride can lead to serious health issues like severe fluorosis, nerve damage, limb dysfunction, body bone and joint deformation, and, in extreme cases, paralysis [2, 3]. Around 200 million people worldwide consume water with fluoride concentrations substantially higher than 1.5 mg/L, the World Health Organization's (WHO) recommended limit [4-6]. In groundwater, a vital source of potable water for many, fluoride concentrations can reach up to 10 mg/L due to the natural dissolution of fluoride-bearing minerals [7]. This high concentration poses a significant health risk. Consequently, developing efficient and affordable methods to remove fluoride from groundwater is crucial, especially in rural areas where small communities lack access to basic water treatment facilities [8].

Adsorption is one of the most common methods used to remove F^- from water, due to its intrinsically low system cost and facile operation [9, 10]. Various inorganic materials including hydroxyapatite [11], zeolite [12], limestone [13], and calcite [14] have all proven effective in the removal of F^- from diverse sourcewaters in previous studies. Hydroxyapatite has achieved a F^- uptake of 15.97 ± 0.03 mg/g after 864 hours of operation, and zeolite composites have shown adsorption capacities of 5.44-10.5 mg/g over pH from 3 to 7. Although nano-sized adsorbents have shown enhanced adsorption performance as a result of their large surface area-to-volume ratios and high reactivities [15, 16], tiny particles are not necessarily suitable for practical applications due to the difficulties associated with their regeneration and reuse [17]. Consequently, adsorbent immobilization technologies have been developed, including various fluidized- and fixed-bed

systems. Among them, electro-sorption using a fixed bed is often considered one of the most promising technologies.

Capacitive deionization (CDI), also commonly referred to as electro-adsorption, is an emerging electrochemical technology that harnesses porous electrodes to preferentially remove charged species from solutions [18, 19]. Compared to conventional adsorption methods, CDI can significantly enhance the removal kinetics of porous electrodes and enable regeneration of the products using a simple discharge stage. CDI has exhibited great potential as a feasible alternative for desalination, and has recently been used to remove a series of harmful contaminants from various sourcewaters. These include fluoride [20-23], arsenic [24], and nitrate [25]; however, conventional CDI most frequently employs porous carbon electrodes that suffer from extremely low removal efficiencies for specific ionic species because of the competitive adsorption characteristics of other co-existing ions in natural sourcewaters. For example, when used for F^- removal, major concerns arise from the substantial differences in anion ratios between fluoride (2–10 mg/L) and other co-existing anions, such as chloride (50–500 mg/L). In addition, fluoride ions have a larger hydrated radius (0.352 nm) and reduced mobility ($1.48 \times 10^{-9} \text{ m}^2 \text{ s}^{-1}$) than chloride ions (0.332 nm and $2.03 \times 10^{-9} \text{ m}^2 \text{ s}^{-1}$) [26], which often leads to the favourable removal of chloride over fluoride in conventional CDI [27].

To enhance the selectivity of CDI under these operating conditions, several functional materials with a unique affinity towards target ions have been tested at the electrode [28]. These include bismuth for Cl^- recovery [29] and lambda- MnO_2 for Li^+ production [30]. In addition, studies have found that functional materials with pseudo-capacitive properties may be able to improve the specific capacity of CDI electrodes [28]. Cerium dioxide (CeO_2) has been suggested as a potential adsorbent for fluoride, with the maximum adsorption capacity of fluoride on CeO_2

nanorods reaching upwards of 71.5 mg/g [31]. In the competing anion-coexisting system, a F^- removal capacity of 32.2 mg/g was obtained by a $CeO_2@SiO_2$ nanocomposite [17]. The strong affinity between F^- and CeO_2 suggest it to be a promising electrode material for the selective removal of fluoride by CDI. However, when combined with the CDI process as the sole electrode material, F^- removal capacity and kinetics can be unsatisfactory due to the limited conductivity of CeO_2 . Moreover, the desorption of F^- from the surface of CeO_2 has proven to be a challenging task due to its high affinity for the ions [32]. Consequently, we propose combining the exceptional affinity of CeO_2 to fluoride with the enhanced electrode conductivity of carbon nanotubes (CNTs) to create a highly efficient, selective, and reversible, point-of-use system for the removal of F^- from diverse types of sourcewaters.

More specifically, in this work, we fabricate CNT-loaded CeO_2 (CNT- CeO_2) electrodes for the selective removal of low-concentration fluoride in complex groundwater mixtures. Electro-sorption measurements were compared across simple standalone CeO_2 electrodes and combined CNT- CeO_2 electrodes to evaluate the removal kinetics, selectivity, stability, and regeneration capabilities of the new functional materials. Electrode characterizations using high-resolution XPS, EPR, and XRD refinement were conducted to reveal the selectivity mechanism of fluoride removal by the CeO_2 electrodes.

2. Materials and Methods

2.1 Chemical Reagents

Cerium chloride·7H₂O (99%, Macklin), citric acid (99.5%, Macklin), sodium hydroxide (95%, Macklin), N-methyl-3-pyridinamine (NMP, 99.9%, Aladdin), polyvinylpyrrolidone (PVDF, MW 400000, Macklin), activated carbon (AC, 400 mesh, Macklin), carbon black (Macklin), sodium fluoride (99.5%, Macklin), sodium chloride (99%, Aladdin) and sodium sulfate (99%, Aladdin) were all used without any further purification. Multiwall carbon nanotubes (CNTs, 10–30 μm in length and 10–20 nm in diameter) were purchased from the XFNANO company, China.

2.2 Preparation of CeO₂ Powder and Electrodes

CeO₂ powder was prepared via the calcination of the precursor Ce(OH)₃, and the synthesis of Ce(OH)₃ was conducted based on methods commonly reported in the literature [33]. CNT-CeO₂ was directly synthesized using the same calcination procedures. The precursors, CNT and Ce(OH)₃, were thoroughly ground together at CNT mass percentages of 10%, 15%, 20%. The resulting products were accordingly referred to as 10-CNT-CeO₂, 15-CNT-CeO₂, and 20-CNT-CeO₂, respectively. Material synthesis details including CeO₂ and a series of CNT-CeO₂ (Text S1) as well as structural and electrochemical characterization (Text S2-S6) are provided in the Supplementary Information. A homogeneous slurry was used for the fabrication of functional anodes, which was prepared by mixing 120 mg of active material (CeO₂ or CNT-CeO₂) with 15 mg of PVDF dispersion as the binder, and 15 mg carbon black in the NMP solvent. The mixture was finally coated on a titanium sheet with a surface area of 5×5 cm², followed by overnight drying at 60 °C in a vacuum oven. The AC electrode was prepared using the same method, prior to being employed as the cathode in all defluoridation experiments.

2.3 Electrochemical Measurements

Electrochemical experiments were tested in a typical three-electrode cell in conjunction with an electrochemical workstation (CHI 660E, China). The active material coated Ti sheet, Pt wire, and Ag/AgCl electrode were used as the working, counter, and reference electrodes, respectively. All electrochemical tests, including electrochemical impedance spectroscopy (EIS), galvanostatic charge-discharge (GCD), and cyclic voltammetry (CV) were carried out using a 0.1 M NaCl solution or a mixed 0.05 M NaCl and 0.05 M NaF solution at room temperature. EIS was performed with an AC voltage of 10 mV at the open circuit potential in a frequency range between 10 mHz to 100 kHz. The specific capacitance (C_s , F/g) of the active materials was determined using the following equation:

$$C_s = \frac{1}{ms\Delta v} \int_{v_0}^{v_0+\Delta v} I dv \quad (1)$$

where m is the mass of active material (g), s is the scan rate (V/s), v_0 is the initial potential, Δv is the potential window of CV, and I is the response current (A).

2.4 Selective Removal of Fluoride

To investigate the electro-adsorption performance of CeO₂ and CNT-CeO₂ electrodes in a batch configuration, a self-circulating system was used, as illustrated in Fig. S1. The system includes a CDI unit cell, an external power supply (2231A-3003, KEITHLEY), and a peristaltic pump. A 50 mL mixed solution of NaF and NaCl (10 mg/L fluoride and 100 mg/L chloride) was used to simulate the fluoride-containing groundwater. During tests, the flow rate and applied voltage were maintained at 15 mL/min and 1.2 V, respectively, and 0.5 mL of sample was withdrawn at different time intervals to determine the remaining concentrations of fluoride and chloride by ion chromatography (IC; AQUION, ThermoFisher). The changes in dissolved oxygen

(DO) content and pH during the fluoride removal process were recorded by the DO meter (Thermo Scientific, ORION STAR A213) and pH meter (Thermo Scientific, ORION STAR A211), respectively. The concentration of potentially released Ce was also recorded using inductively coupled plasma atomic emissions spectroscopy (ICP-AES; iCAP 7000 SERIES, Thermo). The fluoride desorption process was conducted at a potential of -1.2 V and a flow rate of 15 mL/min, while 200 mL of ultrapure water was used as the receiving solution.

During the electro-adsorption process, the kinetic removal rate (k) for fluoride and chloride was regressed to a pseudo-first-order rate equation as follows:

$$-\ln\left(\frac{c_t}{c_0}\right) = kt + b \quad (2)$$

Here, c_0 and c_t represent the initial concentration and the remaining concentration at time t , respectively. The separation factor (φ) of F^-/Cl^- was calculated as follows:

$$\varphi = \frac{c_{F,0} - c_{F,t}}{c_{Cl,0} - c_{Cl,t}} \times 100\% \quad (3)$$

$$\delta = \frac{(c_{F,0} - c_{F,t}) \times V}{m} \quad (4)$$

where the subscripts 0 and t denote the initial and final times, respectively. δ is the removal capacity and V is the volume of solution.

3. Results and Discussion

3.1 Morphology and Structure

SEM images illustrate the morphologies of the electrode materials at different stages of the preparation process. The as-prepared $Ce(OH)_3$ precursor exhibited a nanorod-like morphology (Fig. S2) and was converted to aggregated CeO_2 particles (Fig. 1a-b) during the calcination process.

The addition of the CNTs enabled interspersed nanotubes between the CeO₂ particles to alleviate the aggregation of CeO₂ during the calcination stage (Fig. 1c,1d and Fig. S3). Consequently, compared to the unmodified pristine CeO₂, the specific surface area of the CNT-CeO₂ was substantially higher, with an approximate area increase of 54% (Fig. 1e). In addition, hysteresis loops can be observed in the typical VI isotherm curves for both the pristine CeO₂ and CNT-CeO₂, indicating the existence of mesopores with an average pore size of about 3.5 nm. The presence of additional mesopores with 30.6 nm pore size in CNT-CeO₂ supports the claim that CNTs may decrease the aggregation of CeO₂ (Fig. S4a-b). Furthermore, three types of lattice fringes were observed in the HRTEM image (Fig. S5). The interplanar spacing noted was (i) 0.31 nm, (ii) 0.27 nm, and (iii) 0.19 nm, which were attributed to the (111), (200), and (220) planes of the cubic CeO₂, respectively [34]. XRD patterns (Fig. S6) indicated that the prepared CeO₂ exhibited the characteristic peaks of typical cubic CeO₂ [35]. For the CNT-CeO₂ sample, although the peak intensity was seen to decrease slightly, the characteristic peaks of the pristine CeO₂ were maintained. Although the low loading mass led to the disappearance of the two characteristic peaks of the CNTs in the XRD patterns, the D band (1336 cm⁻¹) and G band (1582 cm⁻¹) of the CNTs could be detected in the Raman spectra [36]. The D and G bands observed were caused by structural defects and hybridized C atoms, respectively (Fig. 1f). The Raman spectra of CNT-CeO₂ maintained these two characteristic peaks, verifying the presence of CNTs.

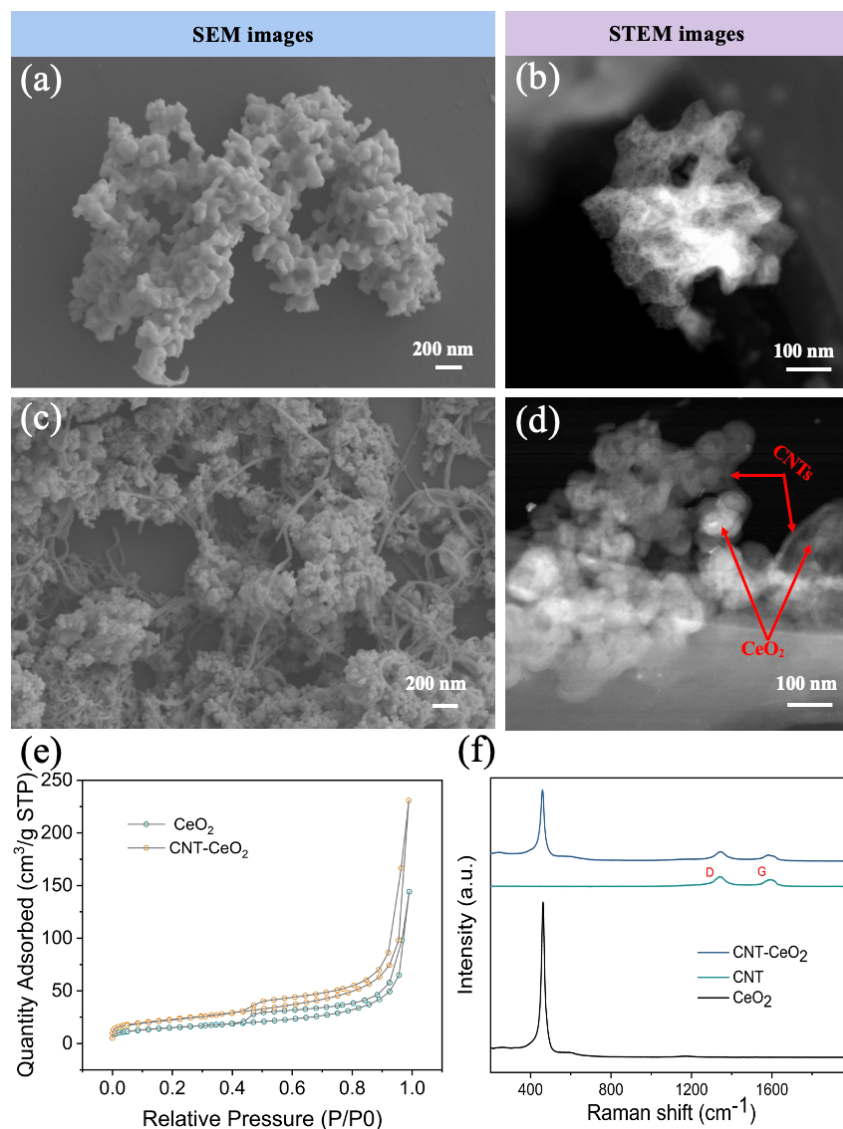


Fig. 1. Morphology and structure characterizations of CeO_2 and CNT-CeO_2 : (a) SEM image and (b) STEM image of CeO_2 ; (c) SEM image and (d) STEM image of CNT-CeO_2 ; (e) nitrogen adsorption-desorption curves and (f) Raman spectra of the CNT, CeO_2 , and CNT-CeO_2 .

3.2 Electrochemical Performance

To understand the interactions between CeO_2 and F^- , as well as the role of the CNTs, we conducted an electrochemical performance study involving three types of electrodes: CeO_2 , CNT, and CNT-CeO_2 . These electrodes were examined in 0.1 M NaCl or a mixed solution containing 0.05 M NaCl and 0.05 M NaF. When the electrodes were submerged into the 0.1 M NaCl solution,

all three electrodes exhibited CV curves with a quasi-rectangular shape (Fig. 2a), indicating excellent double-layer capacitive behaviour, with the corresponding specific capacitance values provided in Fig. S7. Specifically, standalone CNTs displayed the highest specific capacitance with a value of 5.52 F/g, which can be attributed to the superior electrical properties inherent to carbon materials. The hybrid CNT-CeO₂ electrode exhibited a substantially larger calculated specific capacitance (5.16 F/g) than the standalone CeO₂ electrode (3.48 F/g), which could be attributed to the lower aggregation extent and improved wettability of the CNT-CeO₂ electrode in the aqueous system (Fig. S8). Collectively, these results suggest that the CNT-CeO₂ electrode possesses a significantly higher capacity for ion capture, given that larger specific material capacitances typically correspond to improved charge storage capabilities.

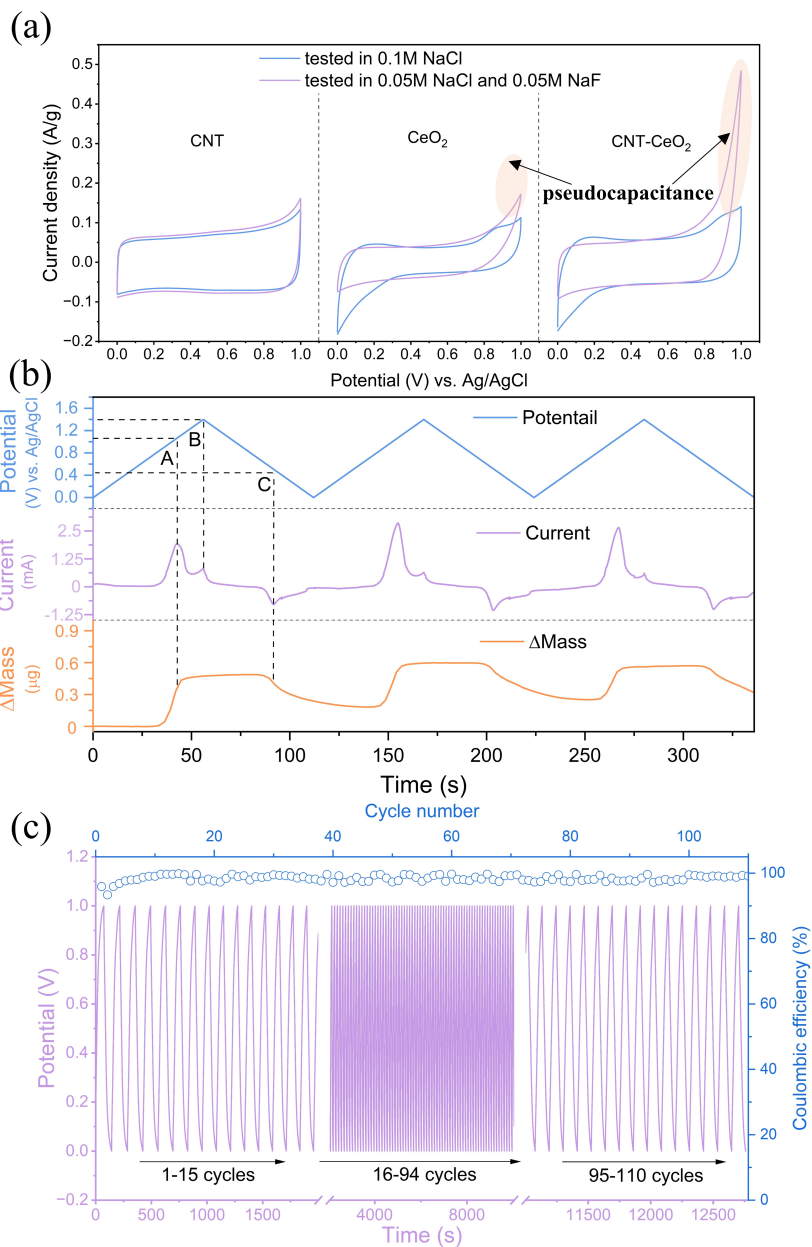


Fig. 2. Electrochemical performance comparisons of CNT, CeO₂, and CNT-CeO₂ electrodes: (a) CV curves of CNT, CeO₂, and CNT-CeO₂ in 0.1 M NaCl solution and a mixed solution of 0.05 M NaCl and 0.05 M NaF; (b) three CV cycles of a CNT-CeO₂ loaded QCM sensor in a mixed solution of 0.05 M NaCl and 0.05 M NaF. (c) GCD cycle curves (110 cycles) and corresponding Coulombic efficiency of CNT-CeO₂.

When the electrolyte was switched to the mixed solution containing 0.05 M NaCl and 0.05

M NaF, only the CeO₂ and CNT-CeO₂ electrodes possessed a Faraday current beyond 0.8 V vs.

Ag/AgCl (Fig. 2a), which may be a by-product of the intercalation Faraday capacitance, also known as the pseudo-capacitance, initiated by the reaction between F^- with CeO_2 . To confirm the presence of the pseudocapacitive effect, we employed electrochemical quartz crystal microbalance (EQCM) to monitor the *in situ* mass and current variations of a CNT- CeO_2 electrode during a CV test. The results, as presented in Fig. 2b, clearly demonstrate a substantial increase in both mass and current as the potential increased beyond 0.8 V vs Ag/AgCl. The concurrent rise in mass and current implies that the surge in current did not arise from water splitting but was predominantly attributed to the adsorption of F^- onto the CNT- CeO_2 electrode. As a result, the current peak A (as indicated in Fig. 2b) at ~1 V represents the redox current arising from the pseudocapacitance region. As the potential continued to rise from 1.2 V to 1.4 V vs Ag/AgCl, an additional peak (peak B) in the current appeared, whereas the mass of the electrode did not change significantly. This observation indicated that the current variation was caused by water oxidation. It is also noteworthy that a simultaneous decrease in mass and increase in reverse current (Peak C) were observed when the potential was lowered to 0.4 V vs Ag/AgCl, implying that the sorption of fluoride by CeO_2 -based electrode is reversible to some extent. Moreover, the pseudo-capacitance of the CNT- CeO_2 was substantially larger than that of the standalone CeO_2 (Fig. 2a), suggesting that CNT- CeO_2 was more feasible for the reaction with F^- . This enhanced performance can be attributed to the more dispersed CeO_2 exposed at the solution-electrode interface as a result of the intercalation of CNTs.

Additionally, we employed EIS to characterize a series of CNT- CeO_2 materials, aiming to acquire direct evidence of their ability to enhance conductivity. As depicted in Fig. S9, CeO_2 alone demonstrates a linear segment in the low-frequency domain, lacking the semicircular feature typically observed in the high-frequency regime. This absence suggests a relatively elevated

inherent resistance in CeO_2 , attributed to its intrinsic semiconductor properties, which subsequently lead to poor conductivity. However, upon incorporation of CNTs, the samples exhibit a semicircular pattern in the high-frequency range. Further, as the loading of CNTs increases, the diameter of the semicircular pattern diminishes, indicating a progressive improvement in the sample's conductivity. Furthermore, assessing cycling stability is a crucial criterion for evaluating the long-term viability of electrode materials in practical applications. This assessment is exemplified by the GCD plots shown in Fig. 2c, where the curves maintained their initial shape with little change even after 110 cycles. Additionally, the Coulombic efficiency of the electrodes consistently exceeds 95%, underscoring the outstanding durability of the CNT- CeO_2 electrodes and their suitability for repeated use and recycling.

3.3 Selective Removal Performance

To study the fluoride electro-adsorption performance of the CeO_2 and the CNT- CeO_2 electrodes, an asymmetric CDI system was built using functional CeO_2 -based electrodes and AC as the anode and cathode, respectively. Additionally, a symmetric AC/AC system was selected as a reference. A mixed solution of NaCl and NaF containing 10 mg/L F^- (equivalent to 0.53 mM) and 100 mg/L Cl^- was used to simulate fluoride and chloride co-existing conditions in groundwater. As shown in Fig. 3a, when traditional AC electrodes were subjected to an applied voltage of 1.2 V, Cl^- was preferentially removed over F^- due to the smaller hydration radius and faster mobility of Cl^- [26]. The concentration of F^- slightly decreased from 10 to ~9 mg/L during a 50-minute experiment, resulting in a very low F^-/Cl^- separation factor of below 0.1. This implies that AC was an inefficient material for selective fluoride separation and removal in the presence of chloride. In contrast, the CeO_2 electrode could continuously and stably reduce the F^- concentration from 10

mg/L down to 1.5 mg/L within 300 min, while Cl^- removal was insignificant. The F^-/Cl^- separation factor of CeO_2 was as high as 3.91 ± 0.24 , indicating that the CeO_2 electrode displayed effective and selective removal for fluoride. We also investigated the effect of the applied voltage on the electro-adsorption efficiency of the CeO_2 electrode by varying the applied voltage between 0 and 1.5 V (Fig. S10). While higher voltages often improve transport kinetics, they can also lead to excessive adsorption of Cl^- ions, resulting in a decrease in the separation factor. Consequently, the optimized working voltage was set to 1.2 V for all subsequent studies, unless otherwise specified.

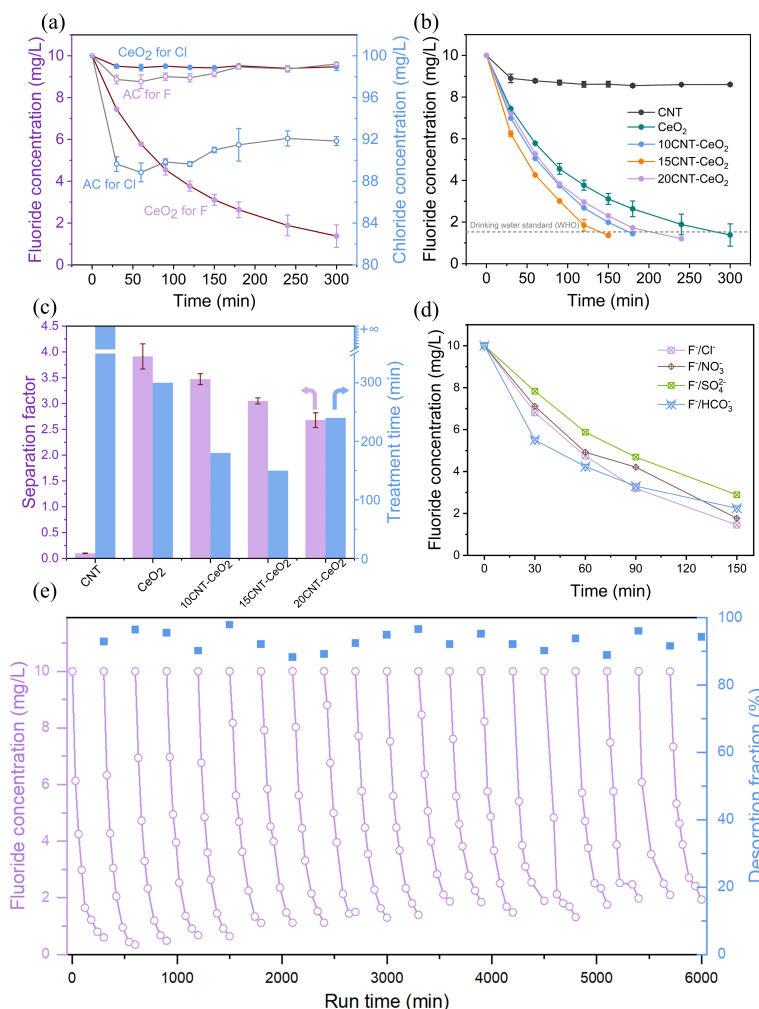


Fig. 3. Selective fluoride removal performance in CDI: (a) fluoride and chloride removal kinetics using the CeO_2 as compared to AC electrodes; (b) fluoride removal kinetics; (c) F^-/Cl^- separation factor and treatment time using the CeO_2 , CNTs, and CNT- CeO_2 electrodes; and (d) selective fluoride removal performance of

the CNT-CeO₂ electrode in the presence of 100 mg/L Cl⁻, NO₃⁻, SO₄²⁻, and HCO₃⁻, respectively; (e) regeneration ability of CNT-CeO₂ electrode in the 20-cycle charge-discharge tests.

The incorporation of CNT with CeO₂ has significant implications for the selective removal of fluoride, and exhibits CNT mass-dependent variations in removal kinetics, separation factors, and removal capacities. Relative to standalone CeO₂, the CNT-CeO₂ electrodes exhibited substantially higher F⁻ removal kinetics (Fig. 3b and Fig. S11), with the highest removal rate achieved by 15-CNT-CeO₂ (15% CNT) at a voltage of 1.2 V, which could be attributed to enhanced electrical conductivity by CNT doping. Higher levels of CNT doping would, however, decrease the F⁻ removal rate, which was potentially caused by the preferable adsorption of chloride over fluoride on the CNTs. Consequently, for 15-CNT-CeO₂, the *k* value reached an impressive 0.7748 h⁻¹, which was 77 times higher than that of standalone CNT (0.0100 h⁻¹). This value also surpassed the rates observed for 10-CNT-CeO₂ (10% CNT) and 20-CNT-CeO₂ (20% CNT), which were 0.6301 and 0.5188 h⁻¹, respectively. It is important to note that 15-CNT-CeO₂ achieved the reduction of F⁻ concentration below the WHO standard of 1.5 mg/L in just 150 min, which is only half the time required using the CeO₂ electrode. Additionally, the CNT loading also enhanced the total F⁻ removal capacities (Fig. S12). In the solution containing 50 mg/L F⁻, the standalone CeO₂ electrode exhibited the lowest adsorption capacity of 10.09 mg/g, while the 10%, 15%, and 20% CNT doped CeO₂ improved the incremental capacity to 13.10, 13.59, and 15.09 mg/g, respectively. The removal capacity in the CDI configuration is typically associated with the number of exposed active sites in the electrodes. Thus, the hindered aggregation by CNT doping likely contributes to the overall increase in fluoride removal capacity.

The F⁻/Cl⁻ separation factor was found to be inversely correlated with the mass percentages of CNTs in the composite electrode. Specifically, the F⁻/Cl⁻ separation factors decreased to 3.47 ±

0.11, 3.05 ± 0.06 , and 2.68 ± 0.14 , when the CNT doping percentages increased to 10%, 15%, and 20%, respectively. The reduced separation factor in the high CNT doping case could be caused by the favorable adsorption of Cl^- by the CNT (Fig. 3c). Excess CNT doping would increase chloride removal and thereby compromise the selective removal of F^- , as evidenced by the low F^-/Cl^- separation factor in the 20-CNT- CeO_2 electrode. This trade-off effect between kinetics and selectivity resulted in 15-CNT- CeO_2 requiring the shortest treatment time to meet 1.5 mg/L standard, with a duration of 150 min, as compared to 300, 180, and 240 min required by CeO_2 , 10-CNT- CeO_2 , 20-CNT- CeO_2 , respectively. In the following investigations, the 15-CNT- CeO_2 was used unless stated otherwise. In addition, we compared the fluoride removal capacities and separation factors of our CeO_2 -based electrodes with those reported in the literature, as shown in Fig. S13 and Table S1. These findings speak to the value of our fabricated CeO_2 -based electrodes for selective fluoride removal. To further evaluate the selectivity of the CNT- CeO_2 electrode, we conducted four control experiments, each containing fluoride in combination with HCO_3^- , SO_4^{2-} , NO_3^- , or Cl^- at a concentration of 100 mg/L. The CNT- CeO_2 electrode exhibited negligible adsorption to NO_3^- and Cl^- and the removal kinetics of fluoride were not affected (Fig. S14 and 3d). Although a small fraction of SO_4^{2-} and HCO_3^- was removed concurrently with fluoride ions, the fluoride removal kinetics were only slightly diminished. However, even under the interference of various high-concentration anions, the removal of F^- could still meet the WHO standard requirements.

CNT- CeO_2 electrodes also exhibited superior F^- desorption performance over standalone CeO_2 (Fig. S15). The F^- desorption efficiency of the CNT- CeO_2 electrode reached ~88-98% after 240 min under -1.2 V and an additional 5 min at 1.2 V to free the sorbed F^- on the counter-electrode AC. This desorption efficiency was nearly twice that of the standalone CeO_2 electrodes. This

enhanced performance can also be attributed to the lower aggregation level of CeO₂ caused by CNT doping. Reduced aggregation of CeO₂ facilitates the release of F⁻ from lattice given the shorter longitudinal moving distance. This is supported by CV curves tested in the voltage range from -1 V to 1 V (Fig. S16): the higher desorption peak intensity of the CNT-CeO₂ electrode at -0.48 V indicates a greater number of ions released from the CNT-CeO₂ electrode compared to the standalone CeO₂ electrode. These results also suggest that the CNTs assist in the desorption of F⁻ from CeO₂, likely ascribed to the elevated conductivity of the electrode with the addition of the CNTs. Technically, the resistance of CeO₂ would cause a drop in the potential on the electrode from the applied voltage. However, the CNT addition eliminates the hindrance, resulting in a higher potential for composite electrodes than the CeO₂ electrode. For the CeO₂ electrode, the defluorination efficiency was about 50% at -1.2 V. However, applying a voltage of -1.4 V achieved ~90% desorption efficiency in 4h (Fig. S17). This implies that the fluoride ion can be almost completely desorbed on the surface of the CeO₂ electrode by increasing the voltage. The satisfactory desorption on either CNT-CeO₂ or CeO₂ electrode suggested that the adsorption-desorption reactions of F⁻ by CeO₂ are mostly reversible.

To investigate the chemical stability of the CNT-CeO₂ electrode, we monitored the concentration of Ce potentially released into the electrolyte solution during the 9-hour CDI process (Fig. S18). The results showed that no Ce was released from the surface of the electrode during either the charging or discharging processes, which indicated the excellent chemical stability of CNT-CeO₂ electrodes. To explicitly demonstrate the reversibility and stability, a 20-cycle experiment using the CNT-CeO₂ electrode was conducted, as shown in Fig. 3e. In this experiment, the kinetics of the 20 cycles and the corresponding desorption fraction of each cycle were recorded. The desorption percentage consistently ranged between 88% and 98%, demonstrating excellent

cycle stability. Furthermore, after 100 hours of operation, the fluoride concentration could still be reduced from an initial 10 mg/L to ~ 1.5 mg/L after the 20th cycle. Subsequently, the electrode was subjected to XPS characterization after 20 cycles, revealing that no signal of F^- could be detected on the surface of the CNT-CeO₂ electrode. This verification confirms that F^- was completely desorbed from the CeO₂ surface (Fig. S19). The recyclability assessment of CeO₂ was also conducted by a 10-cycle charge-discharge test, as presented in Fig. S20. Overall, these tests demonstrate the high stability and reversibility of this CeO₂-based CDI system.

3.4 Practicality and Scalability

To explore the practical potential and scalability of this approach, we set up three parallel sets of amplified CDI devices (Fig. 4a) for fluoride removal experiments. Each set consisted of two large 25×25 cm² electrodes, one employing CNT-CeO₂ and the other using AC, as shown in Fig. 4b. To evaluate the selective F^- removal performance of the CNT-CeO₂ electrodes in complex natural source waters, we chose 4 L of groundwater from Dapeng Bay, Shenzhen, China, as the feed solution. This volume was 80 times larger than the original setup, and the specific compositions of this groundwater are detailed in Table S2. As shown in Fig. 4c and 4d, the CNT-CeO₂ electrodes effectively reduced fluoride concentration from 5.2 mg/L to about 1.4 mg/L, falling below the WHO standard, after a 10-hour operation. In contrast, the residual concentrations of other interfering ions (Cl^- , SO_4^{2-} , and NO_3^-) remained significantly high, with the removal efficiencies of 2.6%, 18.6%, and 26.1%, respectively. These findings reaffirm the selectivity of the CNT-CeO₂ electrodes for removing fluoride from practical, intricate source waters. Additionally, to evaluate the removal kinetics, we've consolidated relevant literature and our findings in Table S3.

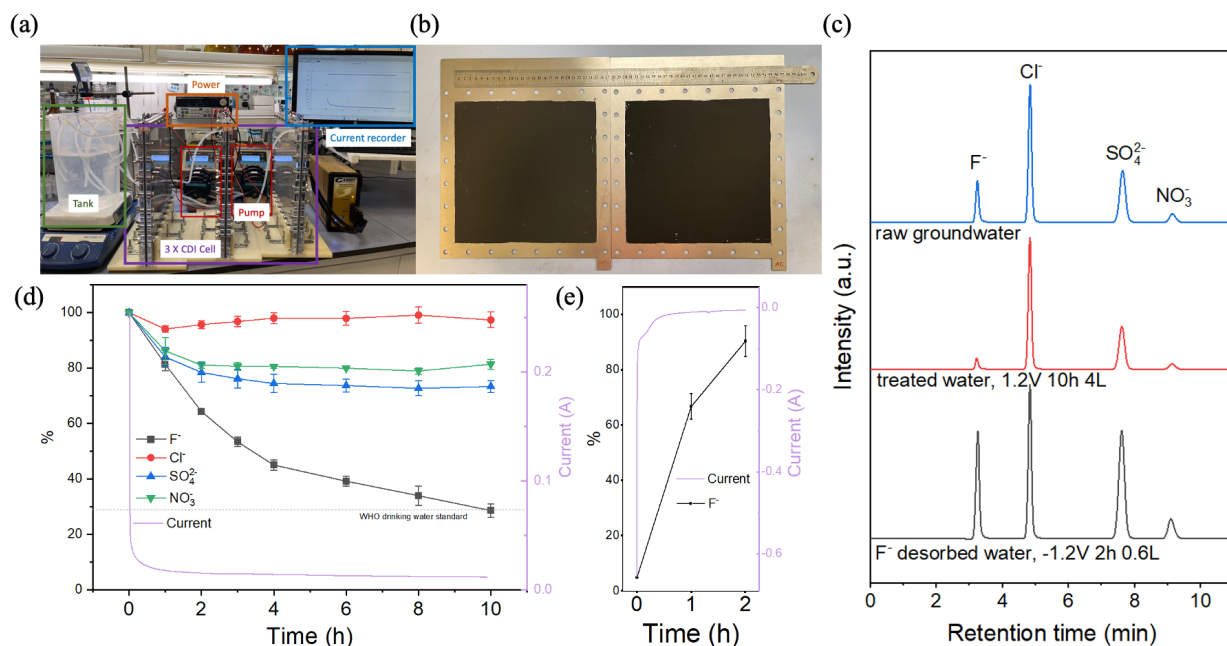


Fig. 4. Scaled-up CDI device and its performance for selective fluoride removal: (a) photographs of the 3×CDI system and (b) a pair of electrodes from one cell; (c) IC spectra data collected from a complete adsorption-desorption cycle; performance of fluoride removal in 4 L of raw groundwater (d) and regeneration in 0.6 L of treated water (e).

Our regeneration process adopted a practical approach: we halted the pump after the fluoride removal process and initiated a reversal under -1.2 V using the retention solution (about 200 mL each) [37]. The results, as illustrated in Fig. 4e, reveal an impressive release of nearly 90% of fluoride ions into the retention solution, indicating substantial regeneration efficiency and water recovery (85%). Moreover, our apparatus allows for two operational cycles within a 24-hour period, resulting in the production of a sufficient 6.8 L of purified water to meet the daily drinking needs of a four-person household. An energy consumption analysis (listed in Test S5) reveals that the energy consumption of groundwater fluoride removal, encompassing defluorination and regeneration process, stands at about 0.20 kWh/m³. Notably, this energy cost is lower than that of alternative fluoride removal technologies, such as electrocoagulation (0.47 kWh/m³) [38], electrodialysis (0.46 kWh/m³) [39], combined electrocoagulation and electroflotation (1.2 kWh/m³)

[40], and nanofiltration (0.4 kWh/m³) [41]. Furthermore, with additional scaling up, the cost of our approach could potentially decrease even further.

3.5 Mechanism of Selective Fluoride Removal

The selectivity mechanism of using CeO₂ as an adsorbent for fluoride removal is still up for debate across the literature. Various mechanisms have been reported in previous studies: (i) ion exchange of fluoride with hydroxyl groups on the CeO₂ surface [42, 43]; (ii) adsorption by CeO₂ surface and Ce³⁺-included O defect [31]; and (iii) -O²⁻ replaced by fluoride [32]. To determine the underlying mechanism responsible for the heightened selectivity, a series of characterizations were conducted including XPS, EPR, and Le Bail refined XRD. Fig. 5a demonstrates a symmetric peak assigned to F 1s appearing in the XPS spectra of the CeO₂ after fluoride electro-sorption, in alignment with the successful immobilization of F⁻ by the electrode surface. In addition, the Ce 3d XPS spectra clearly revealed two chemical states involving Ce³⁺ and Ce⁴⁺ in Fig. 5b [44], and deconvolution analysis indicates that the Ce³⁺/Ce⁴⁺ ratio increased from 20.3% to 25.9% after fluoride adsorption, implying that a portion of Ce⁴⁺ on the CeO₂ electrode surface was converted to Ce³⁺ [45, 46]. The O 1s XPS spectra showed four chemical states of oxygen, including O-Ce⁴⁺, O-Ce³⁺, -OH, and adsorbed H₂O at 529.5, 531.1, 532.3, and 533.2 eV, respectively. It is worth noting that the atomic ratio of O-Ce⁴⁺/ O-Ce³⁺, representing lattice oxygen and oxygen vacancies, respectively, dropped from 1.5 to 0.73 after adsorbing the fluoride ions. The change of Ce valence and reduced percentage of lattice oxygen may be attributed to the partial replacement of the lattice oxygen bonded with the Ce atoms by the adsorbed fluoride. When a lattice oxygen (-O²⁻) was repelled from CeO₂ and became oxygen molecule (O₂), two electrons were released from the vacancy site of CeO₂ and eventually enabled the reduction of Ce⁴⁺ to Ce³⁺ [47-49]. Consequently,

the lattice oxygen was replaced by the fluoride ions, and meanwhile more OH^- ions and H_2O molecules were adsorbed by the unsaturated sites, thereby increasing the adsorption oxygen content as shown in Fig. 5c. Additionally, we carried out EPR measurements to evaluate the defect state of the CeO_2 before and after fluoride adsorption. As shown in Fig. S21, due to the existence of unpaired electrons in CeO_2 , there were Ce^{3+} , O_2^- , and $\text{Ce}^{3+}\text{-O}^-\text{-Ce}^{4+}$ type defect sites [50, 51]. A stronger $\text{Ce}^{3+}\text{-O}^-\text{-Ce}^{4+}$ signal can be detected after the adsorption of fluoride, which may be caused by the conversion of $\text{Ce}^{4+}\text{-O-Ce}^{4+}$ to $\text{Ce}^{3+}\text{-O-Ce}^{4+}$, in accordance with the results of O 1s XPS spectra.

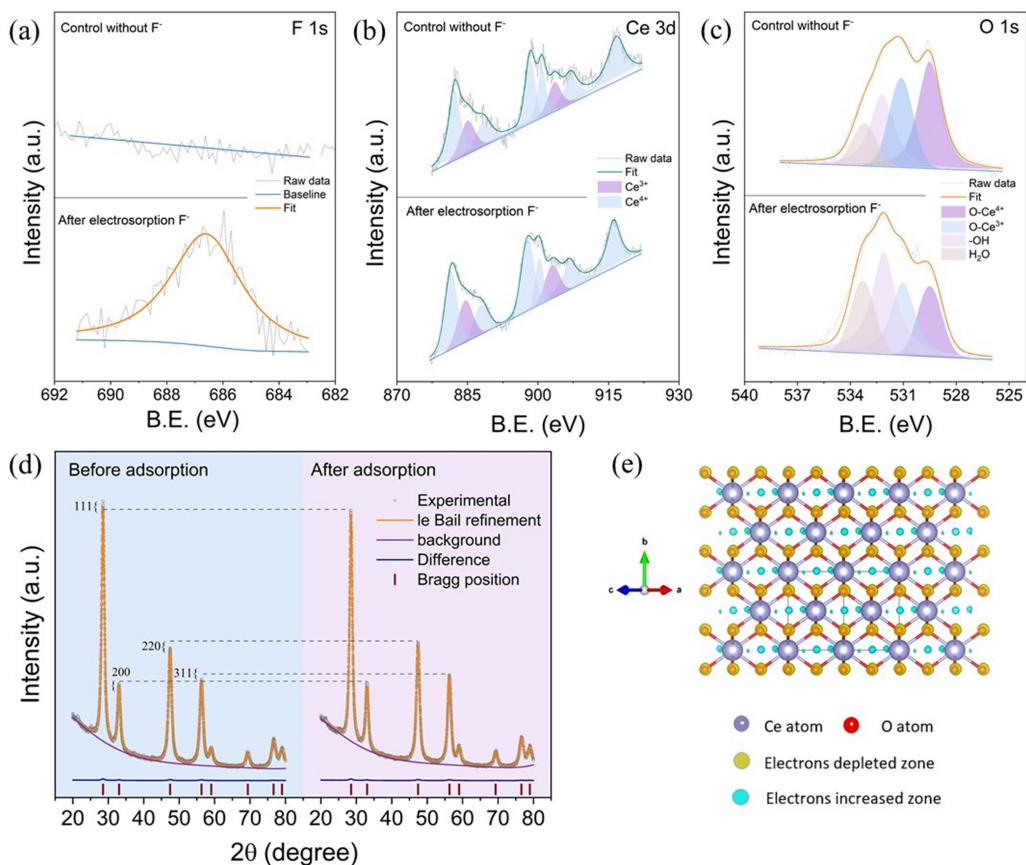


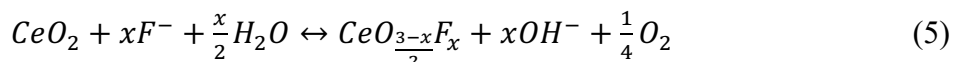
Fig. 5. Mechanism of selective fluoride electro-sorption by CeO_2 : (a) F 1s, (b) Ce 3d, and (c) O 1s high-resolution XPS spectra of the CeO_2 before and after fluoride electrosorption; (d) Le Bail refined XRD spectra before and after adsorption; (e) the electron density profile of fluoride in CeO_2 unit cells ((110) direction).

Le Bail refinement is an advanced technique that can be used to explore foreign atoms in materials systems, relying on precise and quantitative XRD measurement of each facet before and after adsorption, which can reflect electron intensity changes [52]. As shown in Fig. 5d, the intensities of (111) and (200) peaks in the CeO₂ sample after fluoride adsorption were lower than those of pristine CeO₂, but the other peaks exhibited the opposite trend. The obtained XRD data was simulated with refinement and expressed by appropriate functions [53]. Electron density profiles derived from the XRD spectra via sets of Equations (Equation S5) showed that compared to pristine CeO₂, the void space in the CeO₂ lattice exhibited an electron-increased zone after fluoride adsorption, whereas the lattice oxygen sites were electron-depleted (Fig. 5e and S22). Such an electron intensity variation clearly indicates the most electronegative F enters into the lattice of CeO₂ and renders the formation of O defects and thus decreased electron intensity relative to those in the pristine CeO₂.

In addition, we conducted a control experiment, where Ce(OH)₃ was used as the anode in the CDI system. The results are shown in Fig. S23 and illustrate the reduced kinetics and capacity of Ce(OH)₃ relative to standalone CeO₂. These results eliminated the possible mechanism of hydroxyl-exchange, as previously mentioned in the CDI configuration. Instead, this phenomenon could be attributed to the prepared CeO₂ being a loose crystalline material, as evidenced by the broad XRD FWHM (Fig. S6) and high ratio of Ce³⁺ from XPS (Fig. 5b).

It is important to verify the mechanism through studying pH. However, pH variation during F⁻ adsorption/desorption by the CNT-CeO₂ electrode would be disturbed by the water redox under a bias of 1.2 V, as shown in Fig. S24. To eliminate the interference of the redox reactions of water, we also carried out an additional fluoride adsorption test at a low bias of 0.2 V, at which condition the side reactions would not occur, as shown in Fig. S25. Indeed, the concurrent pH increase with

the decreasing fluoride concentration was observed, which verified the mechanism that fluoride can enter the lattice of CeO₂ and release a certain amount of OH⁻. In the reverse process, F⁻ would be forced to release from the electrode (as shown in Fig. 3e), resulting in the regeneration of ceria and indicating that the proposed electrochemical reaction is highly reversible. To illustrate if the consumption of dissolved oxygen (DO) would hamper the desorption of F⁻, we monitored the DO level during the desorption of F⁻ at -1.2 V, as shown in Fig. S26. At this condition, the DO level in the solution maintained arguably the same, and such an oxygen equilibrium might be achieved by the slow DO consumption in the reverse reaction (Equation 5) and the continuous compensation from the atmosphere in our air-exposed circulation system.



4. Conclusion

Excessive fluoride in drinking water is a global health concern affecting millions of people, particularly in developing countries. In this work, we investigate the use of SCDI technology with CNT-CeO₂ electrodes as a promising alternative for fluoride removal from groundwater to help address these concerns. We demonstrate that the CNT-CeO₂ electrode can selectively remove fluoride from mixed synthetic F⁻/Cl⁻ sourcewaters, as well as real groundwater by harnessing a unique interaction that facilitates the integration of fluoride ions into the CeO₂ lattice, as verified by EQCM and XRD refinement. Our studies illustrate an excellent F⁻/Cl⁻ separation factor up to 4.16, which is 40 times higher than that of conventional AC electrodes. The high selectivity and removal efficiency of fluoride by the CNT-CeO₂ electrode without affecting co-existing ions, such as chloride, provide significant environmental benefits. Our research underscores the compelling

cost-efficiency demonstrated by our process in scaled-up experiments, boasting energy consumptions as low as 0.2 kWh/m³. Lastly, the easy regeneration of fluoride-adsorbed CNT-CeO₂ electrodes presents an opportunity for sustainable water treatment, further reducing the reliance on expensive and energy-intensive treatment processes. By improving access to safe drinking water, SCDI with CNT-CeO₂ electrodes can have a substantial impact on public health and the environment, particularly in areas where fluoride contamination is prevalent.

Declaration of Competing Interest

The authors declare that they have no known competing financial interests or personal relationships that could have appeared to influence the work reported in this paper.

Data availability

Data will be made available on request.

Supplementary Information

Additional information on the experiment and results is available in the Supplementary Information.

Acknowledgments

Financial support was provided by the National Natural Science Foundation of China (22076075) and the Centers for Mechanical Engineering Research and Education at MIT and SUSTech. Danyal would also like to acknowledge financial support provided by a fellowship from the Abdul Latif Jameel World Water and Food Systems (J-WAFS) Lab and fellowship support from the Martin Family Society of Fellows. The authors would like to thank Qing Zhang and Xiyuan Zheng at Sun

479 Yat-sen University for their help on the electrode preparation. The authors acknowledge the
480 assistance of SUSTech Core Research Facilities.

481

482 **References**

- 483 [1] S. Ayoob, A.K. Gupta, Fluoride in Drinking Water: A Review on the Status and Stress Effects, *Critical Reviews in*
484 *Environmental Science and Technology* 36(6) (2006) 433-487. <https://doi.org/10.1080/10643380600678112>.
- 485 [2] P. Li, X. He, Y. Li, G. Xiang, Occurrence and Health Implication of Fluoride in Groundwater of Loess Aquifer in
486 the Chinese Loess Plateau: A Case Study of Tongchuan, Northwest China, *Exposure and Health* 11(2) (2019) 95-107.
487 <https://doi.org/10.1007/s12403-018-0278-x>.
- 488 [3] Y. Li, L. Ma, J. Abuduwaili, Y. Li, S. Abdyzhapar Uulu, Spatiotemporal Distributions of Fluoride and Arsenic in
489 Rivers with the Role of Mining Industry and Related Human Health Risk Assessments in Kyrgyzstan, *Exposure and*
490 *Health* (2021). <https://doi.org/10.1007/s12403-021-00417-5>.
- 491 [4] K. Cherukumilli, C. Delaire, S. Amrose, A.J. Gadgil, Factors Governing the Performance of Bauxite for Fluoride
492 Remediation of Groundwater, *Environ Sci Technol* 51(4) (2017) 2321-2328. <https://doi.org/10.1021/acs.est.6b04601>.
- 493 [5] A. Mamuse, R. Watkins, High Fluoride Drinking Water in Gokwe, Northwest Zimbabwe, *Journal of Water*
494 *Sanitation and Hygiene for Development* 6(1) (2016) 55-64. <https://doi.org/10.2166/washdev.2016.188>.
- 495 [6] WHO, <Guidelines for drinking-water quality, 3rd edition.pdf>, 2008, p. 186.
- 496 [7] H. Mjengera, G. Mkongo, Appropriate Defluoridation Technology for Use in Fluorotic Areas in Tanzania, *Physics*
497 *and Chemistry of the Earth* 28(20-27) (2003) 1097-1104. <https://doi.org/10.1016/j.pce.2003.08.030>.
- 498 [8] Y.D. Ahdab, G.P. Thiel, J.K. Boehlke, J. Stanton, J.H. Lienhard, Minimum Energy Requirements for Desalination
499 of Brackish Groundwater in the United States with Comparison to International Datasets, *Water Res* 141 (2018) 387-
500 404. <https://doi.org/10.1016/j.watres.2018.04.015>.
- 501 [9] J.Y. Su, M.S. Yuan, L. Han, H.X. Deng, J.H. Chang, Y.T. Zhuang, J.Y. Wang, Y. Zhang, Ultrathin Metal Organic
502 Framework Nanosheets with Rich Defects for Enhanced Fluoride Removal, *Chem Eng J* 451 (2023).
503 <https://doi.org/ARTN 13898910.1016/j.cej.2022.138989>.
- 504 [10] Y. Pan, X. Liu, M. Zhang, Q. Han, Y. Shu, M. Wang, B. Liu, Z. Wang, The Impact of Redox Annealing on Intrinsic
505 Properties and Fluoride Adsorption Performance of CeO₂ Nanomaterials, *Chem Eng J* 476 (2023).
506 <https://doi.org/10.1016/j.cej.2023.146347>.
- 507 [11] D.S. Mosiman, A. Sutrisno, R.Q. Fu, B.J. Marinas, Internalization of Fluoride in Hydroxyapatite Nanoparticles,
508 *Environ Sci Technol* 55(4) (2021) 2639-2651. <https://doi.org/10.1021/acs.est.0c07398>.
- 509 [12] J.A. Arcibar-Orozco, A.I. Flores-Rojas, J.R. Rangel-Mendez, P.E. Diaz-Flores, Synergistic Effect of
510 Zeolite/chitosan in the Removal of Fluoride from Aqueous Solution, *Environ Technol* 41(12) (2020) 1554-1567.
511 <https://doi.org/10.1080/09593330.2018.1542033>.
- 512 [13] S. Gogoi, S.K. Nath, S. Bordoloi, R.K. Dutta, Fluoride Removal from Groundwater by Limestone Treatment in
513 Presence of Phosphoric Acid, *J Environ Manage* 152 (2015) 132-139. <https://doi.org/10.1016/j.jenvman.2015.01.031>.
- 514 [14] B.D. Turner, P. Binning, S.L.S. Stipp, Fluoride removal by calcite: Evidence for Fluorite Precipitation and Surface
515 Adsorption, *Environ Sci Technol* 39(24) (2005) 9561-9568. <https://doi.org/10.1021/es0505090>.
- 516 [15] Z. Qu, G. Dong, S. Zhu, Y. Yu, M. Huo, K. Xu, M. Liu, Recycling of Groundwater Treatment Sludge to Prepare
517 Nano-rod Erdite Particles for Tetracycline Adsorption, *Journal of Cleaner Production* 257 (2020).
518 <https://doi.org/10.1016/j.jclepro.2020.120462>.
- 519 [16] Z. Qu, Y. Wu, S. Zhu, Y. Yu, M. Huo, L. Zhang, J. Yang, D. Bian, Y. Wang, Green Synthesis of Magnetic Adsorbent
520 Using Groundwater Treatment Sludge for Tetracycline Adsorption, *Engineering* 5(5) (2019) 880-887.
521 <https://doi.org/10.1016/j.eng.2019.06.001>.
- 522 [17] F. Wang, K.T. Wang, Y. Muhammad, Y.Z. Wei, L. Shao, X.P. Wang, Preparation of CeO₂@SiO₂ Microspheres by
523 a Non-sintering Strategy for Highly Selective and Continuous Adsorption of Fluoride Ions from Wastewater, *ACS*
524 *Sustain Chem Eng* 7(17) (2019) 14716-14726. <https://doi.org/10.1021/acssuschemeng.9b02643>.
- 525 [18] J.Y. Wu, X.X. Xuan, S.H. Zhang, Z. Li, H.L. Li, B. Zhao, H.L. Ye, Z.C. Xiao, X.X. Zhao, X.T. Xu, X.J. Liu, J.
526 You, Y. Yamauchi, N. P-doped Carbon Nanorings for High-performance Capacitive Deionization, *Chem Eng J* 473
527 (2023). <https://doi.org/ARTN 14542110.1016/j.cej.2023.145421>.
- 528 [19] T.K.A. Nguyen, T.V. Huynh, R.A. Doong, Enhanced Capacitive Deionization of Cr(VI) using Functionalized
529 Metal Carbide 2D Framework and Badam Tree Leaf-derived Carbon as the Asymmetric Electrode Materials, *Chem*
530 *Eng J* 475 (2023). <https://doi.org/ARTN 14643910.1016/j.cej.2023.146439>.
- 531 [20] J.-C. Wu, S.S. Chen, T.-C. Yu, K.C.W. Wu, C.-H. Hou, Effective Electrochemically Controlled Removal of
532 Fluoride Ions Using Electrodeposited Polyaniline-carbon Nanotube Composite Electrodes, *Sep Purif Technol* 254
533 (2021) 117561. <https://doi.org/10.1016/j.seppur.2020.117561>.

- [21] W. Tang, P. Kovalsky, D. He, T.D. Waite, Fluoride and Nitrate Removal from Brackish Groundwaters by Batch-mode Capacitive Deionization, *Water Res* 84 (2015) 342-349. <https://doi.org/10.1016/j.watres.2015.08.012>.
- [22] G.Z. Wang, T.T. Yan, J.J. Shen, J.P. Zhang, D.S. Zhang, Capacitive Removal of Fluoride Ions via Creating Multiple Capture Sites in a Modulatory Heterostructure, *Environ Sci Technol* 55(17) (2021) 11979-11986. <https://doi.org/10.1021/acs.est.1c03228>.
- [23] A. Epshtein, O. Nir, L. Monat, Y. Gendel, Treatment of Acidic Wastewater via Fluoride Ions Removal by SiO₂ Particles Followed by Phosphate Ions Recovery Using Flow-electrode Capacitive Deionization, *Chem Eng J* 400 (2020). <https://doi.org/ARTN 12589210.1016/j.cej.2020.125892>.
- [24] D.V. Cuong, P.C. Wu, S.Y.H. Liou, C.H. Hou, An Integrated Active Biochar Filter and Capacitive Deionization System for High-performance Removal of Arsenic From Groundwater, *J Hazard Mater* 423 (2022). <https://doi.org/10.1016/j.jhazmat.2021.127084>.
- [25] D.I. Oyarzun, A. Hemmatifar, J.W. Palko, M. Stadermann, J.G. Santiago, Ion Selectivity In Capacitive Deionization with Functionalized Electrode: Theory and Experimental Validation, *Water Research X* 1 (2018). <https://doi.org/10.1016/j.wroa.2018.100008>.
- [26] W.W. Tang, P. Kovalsky, B.C. Cao, D. He, T.D. Waite, Fluoride Removal from Brackish Groundwaters by Constant Current Capacitive Deionization (CDI), *Environ Sci Technol* 50(19) (2016) 10570-10579. <https://doi.org/10.1021/acs.est.6b03307>.
- [27] R.K. McGovern, A.M. Weiner, L. Sun, C.G. Chambers, S.M. Zubair, J.H. Lienhard, On the Cost of Electrodialysis for the Desalination of High Salinity Feeds, *Applied Energy* 136 (2014) 649-661. <https://doi.org/10.1016/j.apenergy.2014.09.050>.
- [28] C.Y. Zhang, D. He, J.X. Ma, W.W. Tang, T.D. Waite, Faradaic Reactions in Capacitive Deionization (CDI) - Problems and Possibilities: A review, *Water Res* 128 (2018) 314-330. <https://doi.org/10.1016/j.watres.2017.10.024>.
- [29] J.J. Chang, Y.P. Li, F. Duan, C.L. Su, Y.J. Li, H.B. Cao, Selective Removal of Chloride Ions by Bismuth Electrode in Capacitive Deionization, *Sep Purif Technol* 240 (2020). <https://doi.org/10.1016/j.seppur.2020.116600>.
- [30] Z. Zhang, X. Du, Q. Wang, F.F. Gao, T.T. Jin, X.G. Hao, P.F. Ma, J. Li, G.Q. Guan, A Scalable Three-dimensional Porous Lambda-MnO₂/rGO/Ca-alginate Composite Electroactive Film with Potential-responsive Ion-pumping Effect for Selective Recovery of Lithium Ions, *Sep Purif Technol* 259 (2021). <https://doi.org/10.1016/j.seppur.2020.118111>.
- [31] D.J. Kang, X.L. Yu, M.F. Ge, Morphology-dependent Properties and Adsorption Performance of CeO₂ for Fluoride removal, *Chem Eng J* 330 (2017) 36-43. <https://doi.org/10.1016/j.cej.2017.07.140>.
- [32] U.S. Rashid, T.K. Das, T.S. Sakthivel, S. Seal, A.N. Bezbaruah, GO-CeO₂ Nanohybrid for Ultra-rapid Fluoride Removal from Drinking Water, *Sci Total Environ* 793 (2021). <https://doi.org/ARTN14854710.1016/j.scitotenv.2021.148547>.
- [33] B. Xu, L. Xia, F. Zhou, R. Zhao, H. Chen, T. Wang, Q. Zhou, Q. Liu, G. Cui, X. Xiong, F. Gong, X. Sun, Enhancing Electrocatalytic N₂ Reduction to NH₃ by CeO₂ Nanorod with Oxygen Vacancies, *Acs Sustain Chem Eng* 7(3) (2019) 2889-2893. <https://doi.org/10.1021/acssuschemeng.8b05007>.
- [34] P.S. Murphin Kumar, S. Thiripuranthagan, T. Imai, G. Kumar, A. Pugazhendhi, S.R. Vijayan, R. Esparza, H. Abe, S.K. Krishnan, Pt Nanoparticles Supported on Mesoporous CeO₂ Nanostructures Obtained through Green Approach for Efficient Catalytic Performance toward Ethanol Electro-oxidation, *ACS Sustainable Chemistry & Engineering* 5(12) (2017) 11290-11299. <https://doi.org/10.1021/acssuschemeng.7b02019>.
- [35] J. Wang, Z. Li, S. Zhang, S. Yan, B. Cao, Z. Wang, Y. Fu, Enhanced NH₃ gas-sensing performance of silica modified CeO₂ nanostructure based sensors, *Sensor Actuat B-Chem* 255 (2018) 862-870. <https://doi.org/10.1016/j.snb.2017.08.149>.
- [36] K.-H. Wu, D.-W. Wang, I.R. Gentle, Revisiting Oxygen Reduction Reaction on Oxidized and Unzipped Carbon Nanotubes, *Carbon* 81 (2015) 295-304. <https://doi.org/10.1016/j.carbon.2014.09.060>.
- [37] C. Bales, A.S. Kinsela, C. Miller, Y. Wang, Y.Y. Zhu, B.Y. Lian, T.D. Waite, Removal of Trace Uranium from Groundwaters Using Membrane Capacitive Deionization Desalination for Potable Supply in Remote Communities: Bench, Pilot, and Field Scale Investigations, *Environ Sci Technol* 57(30) (2023) 11345-11355. <https://doi.org/10.1021/acs.est.3c03477>.
- [38] U.T. Un, A.S. Koparal, U.B. Ogutveren, Fluoride Removal from Water and Wastewater with a Bach Cylindrical Electrode Using Electrocoagulation, *Chem Eng J* 223 (2013) 110-115. <https://doi.org/10.1016/j.cej.2013.02.126>.
- [39] S. Lahnid, M. Tahaiht, K. Elaroui, I. Idrissi, M. Hafsi, I. Laaziz, Z. Amor, F. Tiyal, A. Elmidaoui, Economic Evaluation of Fluoride Removal by Electrodialysis, *Desalination* 230(1-3) (2008) 213-219. <https://doi.org/10.1016/j.desal.2007.11.027>.

- [40] Q.H. Zuo, X.M. Chen, W. Li, G.H. Chen, Combined Electrocoagulation and Electroflotation for Removal of Fluoride from Drinking Water, *J Hazard Mater* 159(2-3) (2008) 452-457. <https://doi.org/10.1016/j.jhazmat.2008.02.039>.
- [41] F. Elazhar, M. Tahaikt, A. Achatei, F. Elmidaoui, M. Taky, I. Laaziz, S. Jariri, M. El Amrani, A. Elmidaoui, Economical Evaluation of the Fluoride Removal by Nanofiltration, *Desalination* 249(1) (2009) 154-157. <https://doi.org/10.1016/j.desal.2009.06.017>.
- [42] A. Dhillon, T.K. Sharma, S.K. Soni, D. Kumar, Fluoride Adsorption on a Cubical Ceria Nanoadsorbent: Function of Surface Properties, *Rsc Adv* 6(92) (2016) 89198-89209. <https://doi.org/10.1039/c6ra16962g>.
- [43] S. Nehra, S. Raghav, D. Kumar, Biomaterial Functionalized Cerium Nanocomposite for Removal of Fluoride Using Central Composite Design Optimization Study, *Environmental Pollution* 258 (2020). <https://doi.org/10.1016/j.envpol.2019.113773>.
- [44] L. Chen, R. Lin, X.T. Yu, T. Zheng, M.C. Dong, M.Y. Lou, Y.Y. Ma, Z.X. Hao, Microporous Layer Containing CeO₂-Doped 3D Graphene Foam for Proton Exchange Membrane Fuel Cells at Varying Operating Conditions, *Acs Appl Mater Inter* 13(17) (2021) 20201-20212. <https://doi.org/10.1021/acsami.1c03699>.
- [45] Y. Wang, T. Liu, J. Liu, Synergistically Boosted Degradation of Organic Dyes by CeO₂ Nanoparticles with Fluoride at Low pH, *Acs Appl Nano Mater* 3(1) (2020) 842-849. <https://doi.org/10.1021/acsanm.9b02356>.
- [46] L. Chen, R. Lin, X. Yu, T. Zheng, M. Dong, M. Lou, Y. Ma, Z. Hao, Microporous Layer Containing CeO₂-Doped 3D Graphene Foam for Proton Exchange Membrane Fuel Cells at Varying Operating Conditions, *Acs Appl Mater Inter* 13(17) (2021) 20201-20212. <https://doi.org/10.1021/acsami.1c03699>.
- [47] R. Schmitt, A. Nenning, O. Kraynis, R. Korobko, A.I. Frenkel, I. Lubomirsky, S.M. Haile, J.L.M. Rupp, A Review of Defect Structure and Chemistry in Ceria and Its Solid Solutions, *Chemical Society Reviews* 49(2) (2020) 554-592. <https://doi.org/10.1039/c9cs00588a>.
- [48] T.X.T. Sayle, F. Caddeo, X. Zhang, T. Sakthivel, S. Das, S. Seal, S. Ptasińska, D.C. Sayle, Structure–Activity Map of Ceria Nanoparticles, Nanocubes, and Mesoporous Architectures, *Chem Mater* 28(20) (2016) 7287-7295. <https://doi.org/10.1021/acs.chemmater.6b02536>.
- [49] C.T. Campbell, C.H.F. Peden, Chemistry - Oxygen Vacancies and Catalysis on Ceria Surfaces, *Science* 309(5735) (2005) 713-714. <https://doi.org/10.1126/science.1113955>.
- [50] Y.-F. Sun, J.-J. Li, F. Xie, Y. Wei, M. Yang, Ruthenium-loaded Cerium Dioxide Nanocomposites with Rich Oxygen Vacancies Promoted the Highly Sensitive Electrochemical Detection of Hg(II), *Sensor Actuat B-Chem* 320 (2020). <https://doi.org/10.1016/j.snb.2020.128355>.
- [51] L. Wang, Y. Yu, H. He, Y. Zhang, X. Qin, B. Wang, Oxygen Vacancy Clusters Essential for the Catalytic Activity of CeO₂ Nanocubes for O-xylene Oxidation, *Sci Rep-Uk* 7(1) (2017). <https://doi.org/10.1038/s41598-017-13178-6>.
- [52] S.S. Shang, C. Yang, C.G. Wang, J.S. Qin, Y. Li, Q.F. Gu, J. Shang, Transition-Metal-Containing Porphyrin Metal-Organic Frameworks as pi-Backbonding Adsorbents for NO₂ Removal, *Angew Chem Int Edit* 59(44) (2020) 19680-19683. <https://doi.org/10.1002/anie.202007054>.
- [53] Z. Jiang, X. Xu, Y. Ma, H.S. Cho, D. Ding, C. Wang, J. Wu, P. Oleynikov, M. Jia, J. Cheng, Y. Zhou, O. Terasaki, T. Peng, L. Zan, H. Deng, Filling Metal-organic Framework Mesopores with TiO₂ for CO₂ Photoreduction, *Nature* 586(7830) (2020) 549-+. <https://doi.org/10.1038/s41586-020-2738-2>.